Hyperspectral Imaging of Trench Stratigraphy:
Towards Improving the Recognition and Documentation of Past
Earthquakes at Paleoseismic Sites

Daniel Ragona, Bernard Minster, Yuri Fialko,   UCSD, Thomas Rockwell, SDSU

1   Introduction

We have initiated a pilot project to use hyperspectral imagery to assist in the recognition and documentation of paleoseismic events in trench exposures. In earthquake geology, the success in the identification and description of the stratigraphy of a site conditions the interpretation of the earthquake history of that location. A common problem when working in trench exposures is related to the difficulty of visually identifying unique physical characteristics that define stratigraphic units. Differences in description can result in either an incomplete or misinterpreted earthquake history (McCalpin, 1996; Weldon, McCalpin and Rockwell, 1996). The current method of dealing with this problem is to conduct a multi-investigator review and debate on the exposures and to cut a sufficient number of exposures (trenches) to make sure nothing is missed. Recent advances in hyperspectral imagery suggest that trench stratigraphy could be analyzed in much the same way as LandSat or Aviris imagery of Earth's surface. In principle, hyperspectral images provide a much complete spectral range than the one perceived for the human eye and therefore can be used to elucidate and record physical and chemical characteristics commonly missed in the visual inspection. The use of hyperspectral imagers has two main potential advantages 1) enhance our otherwise limited visual perception and 2) creates an unbiased record of the trench exposure that can be available to the scientific community.

Ultimately, the improvement in the description of the stratigraphic and structural relationships in a trench site will eliminate many of the problems in interpretation of the earthquake history and therefore significantly improve our understanding of earthquakes.

This report describes the methodology adopted as a proof of concept to test the potential of the hyperspectral techniques to properly identify sedimentary units in a trench site. We also report on the notable shortcomings and successes of this experiment.

We conclude that the pilot project demonstrates that the technique offers great promise, especially when using a supervised classification scheme similar to that proposed by Blom et al. (1980) and Krause et al. (1993). We suggest ways to proceed to the next step in developing this approach further.

2   Motivation for a pilot project:

In spite of considerable effort and research we were unable to identify a commercial hyperspectral imager that would be appropriate for our purposes, in terms of resolution, number of bands, and total spectral range. The technology exists, but building a new instrument would cost considerably more than could be justified without a proof-of-concept. On the other hand, several models of portable single-pixel photospectrometers do exist on the market, and are used to calibrate airborne and space borne multi-spectral images. Our strategy therefore focused on collecting a basic data set in an area where the geological interpretation is relatively unambiguous. The purpose is to permit determination of the optimal bands to use, the number of such bands, and the resolution required to improve paleoseismic interpretation. In addition, we would like to characterize the possible impact of a number of parameters, which are not easily controlled in the field, such as illumination, moisture content, etc. Another issue is the need to characterize the variability of the spectra within a single stratigraphic unit.

3   Site Location

The trench site chosen for this study is located at Hog Lake on the Clark segment of the San Jacinto Fault, Riverside County, southern California (Figure 1). We selected this location to take advantage of an ongoing SCEC-funded paleoseismic project at that site and because of its excellent stratigraphy. The study area consisted of five fault-orthogonal trenches excavated at the bottom of Hog Lake, which at the time of the experiment was completely dry. We chose a 50 by 50 cm area on the first exposure of the north wall of trench T 2, between F2 and G2 vertical strings and the middle and lower horizontal strings (Figure 2).
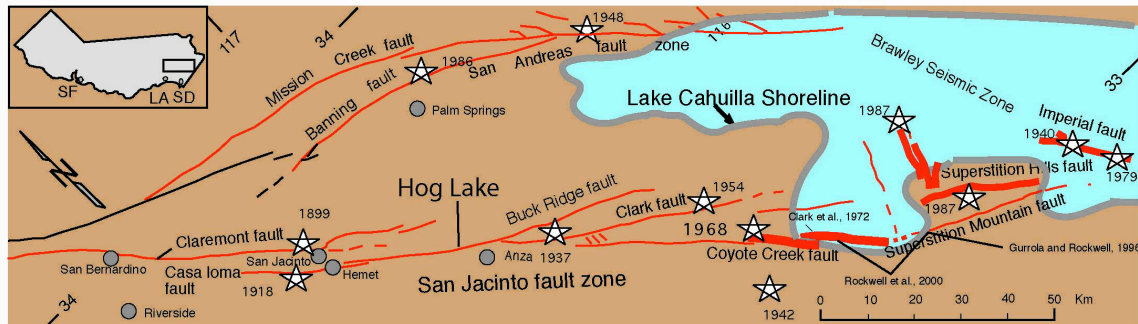

Figure 1. *Location map of the Hog Lake paleoseismological experiment.*

4   Description of the Stratigraphic Section

The sediments collected in the study are dominated by silt-sized clastic sediments derived principally from a granitic source. The local Protolith is mostly tonalite, with minor gabbro and granodiorite.
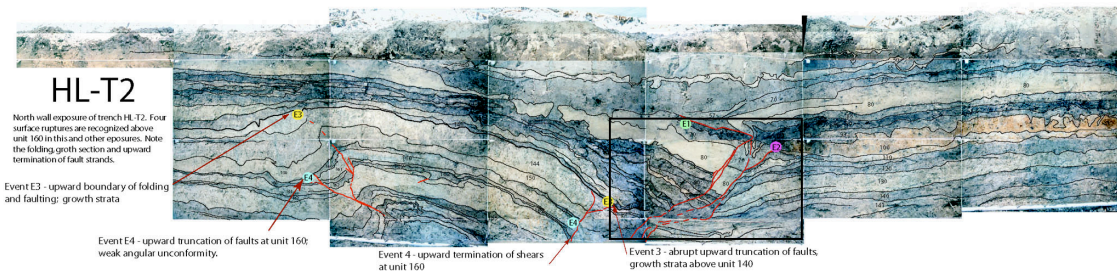

Figure 2*: Trench T-2 and location of the sampling area (black rectangle)*

Silt and very fine sand are the dominant size fractions, but some layers have appreciable clay-sized particles and one unit is a fine micaceous sand.

5   Methodology

Why should we decide to take samples of the trench wall, instead of taking the instrument to the field? We decided to take samples instead of obtaining direct measurements from the trench wall because we wanted to preserve the material for future studies (sedimentological analysis, X ray, etc) and also because our strategy called for data collection under more controlled conditions of light and humidity. In addition, we preferred to avoid, for the time being, the difficulties of operating an expensive instrument in a trench under field conditions.

5.1   Sampling Technique

The experiment was designed to obtain a square matrix of samples that could be used to generate a low-resolution image of the sampled area, in the sense that each sample represents a single

pixel. To perform the sampling, a grid was built in a wooden frame that is attached to the trench face, thereby preserving a reasonably exact location of each sample collected. Sampling cylinders were prepared and a customized sampling box was constructed in order to record the samples in same relative position, as they were collected from the trench wall. A brief description of each of these elements follows.

Figure 3: *North wall of trench T-2 were the box, grid and samples can be seen.*

Sampling grid: a grid of 50 by 100 cm that was built using welded wire mesh with openings of 2.5 by 2.5 cm. (Figure 3). The grid has a total of 800 squares. Each square was identified with a number (horizontal axis, 0 to 39) and a letter (vertical axis, A to T); the mesh was attached to a wooden frame, designed to be placed between the strings of the trench grid.

Sampling cylinders: two types of pipe were used for this purpose; 1.9 cm diameter metallic pipe (3/4 inch electrical conduit) and 1.27 cm PVC pipe (1/2 inch schedule 40 water pipe). Both types were cut in 6 cm long pieces and a number was assigned based on their location in the sampling box (Figure 3). Two hundred of each type were prepared for this experiment. About 50% of the samples ultimately retrieved were housed in metal cylinders, and the other 50% in PVC cylinders.

Sampling box: a square wooden box of 60x60x10 cm was constructed to place the cylinders with the samples (Figure 3). Inside the box, a welded wire mesh of the same type used for the sampling grid was set in order to create a location for each sample. The squares of the mesh were numbered the same as the ones on the sampling grid.

To obtain the samples, we first cleaned an area between vertical strings F2 and G2 and the middle and low horizontal strings in the first exposure of the north wall of trench T-2 (Figure 4).

Figure 4. *Detail of the sampling area between vertical strings F2 and G2.*

After preparation of the wall surface, the sampling grid was placed between the four strings as mentioned above; a small deviation between the vertical strings and the sampling grid could not be corrected in the field (approximately 2.5 cm between the top and the bottom of the grid) but was taken into account to match the sample location with the stratigraphy. Once the grid was set in position, each of the sampling cylinders was placed in one of the squares of the grid and then pushed into the wall, leaving only 1 cm of the cylinder protruding from the wall. The back of the tubes was sealed with expansible foam (Figure 3) to protect the sample from being lost after removing the cylinder from the wall and to retain field moisture content. After the foam dried, we carefully pulled the pipes from the wall in such a way that the sediment was preserved inside the cylinder; each of the samples was numbered and located in the proper place in the sampling box. Using this technique, we took 400 hundred samples located in the rows A to T and columns 10 to 29 (Figure 3).

6   Collection of spectral data from the samples

The samples were taken to the Jet Propulsion Laboratory to obtain the spectral data using a FieldSpec Pro spectroradiometer built by Analytical Spectral Devices, Inc. This procedure was performed in collaboration with Dr. Ronald Blom and Dr. Mark Hemlinger of the Jet Propulsion Laboratory, who spent much time teaching us the basic techniques. The technical specifications of the instrument are specified below. (see http://www.asdi.com/asdi_t2_pr_sp_fsp.html)

   Instrument: FieldSpec® Pro FR, unit 6266 on Calibration 1 with 8° foreoptic.
   Spectral Range: 350-2500 nm
   Spectral Resolution: 3 nm @ 700 nm, 10 nm @ 1400 & 2100nm
   Sampling Interval: 1.4 nm @ 350-1050 nm, 2 nm @ 1000-2500 nm

Scanning time: 100 milliseconds

Detectors: One 512 element Si photodiode array 350-1000 nm.Two separate, TE cooled, graded index InGaAs photodiodes 1000-2500 nm.

Input: 1.4 m fiber optic (25° field of view). Optional foreoptics available

Calibration: Wavelength, reflectance, radiance*, irradiance*. All calibrations are NIST traceable (*radiometric calibrations are optional).

Noise Equivalent Radiance (NeDL): UV/VNIR 1.4 x 10-9 W/cm2/nm/sr @ 700nm NIR 2.4 x 10-9 W/cm2/nm/sr @ 1400nm NIR 8.8 x 10-9 W/cm2/nm/sr @ 2100nm

Weight: 7.2 kg or 15.8 lbs

7   Measurements

The sampling box containing the samples was located over a meter tall table, in bright sunlight. The methodology consisted of the following protocol. First, the gain of the instrument was automatically adjusted by pointing the probe to a reference Lambertian reflector (optimization). Once the optimization was performed, five measurements on the reference Lambertian reflector were obtained (standardization). Then each of the 20 samples in a single row (A to T) were measured five times to test variability and reproducibility. Finally, a new standardization was performed resulting in 110 spectra per row. The procedure was repeated for each row and data saved on disk. Additional readings of the PVC, metal cylinders and rust were performed in order to assess possible contamination of the spectral data.

Finally, we moistened one row and re-measured it following the same protocol, to test the affect of moisture content on the radiometer readings. In all, nearly 2350 individual spectra were collected for analysis.

The data was stored in 24 folders labeled Array 1 to 20 for the measurements corresponding to the samples in the box and ArraysWet,PVC,Metal,Rust for the complementary measurements. Each folder contains binary files corresponding to each of the measurements performed. Array 1 to 20 contains 110 binary files.

8   Data processing

8.1   Raw data

The data saved from the FieldSpec® Pro FR was transformed from binary to ASCII using ViewSpec provided from the same company that built the instrument. Each of the 20 folders corresponding to the samples in the box was transformed into a 2152x111 matrix. The first row is the time of the recording and the first column is the wavelengths. The 2151 bands correspond to the 350 to 2500 wavelengths. Although the bandwidth of the instrument varies between 1.5 nm to 12 nm, the output data is automatically re-sampled at 1 nm. The values stored in these matrices have no units, and are considered DN (digital number) (Figure 5). Ideally the instrument is recording irradiance but since there are several other sources of photons, the values recorded can be far from being irradiance values. In order to compare we have to normalize it to the conditions of incoming light plus electronics at the time of the measurement therefore we needed to transform the values of DN to Reflectance.

8.2   *Reflectance calculation*

the data recorded by the instrument can not be directly compared because it is the result of several time depending factors such as changes in the atmospheric conditions, and other variations that may depend on the instrument. To obtain a spectra that can be easily compared with other measurements performed at different times and atmospheric conditions we needed to normalize our data using the measurements of the Lambertian surface (Spectralon®) that we recorded at the beginning and at the end of each array (box row).

Reflectance is the ratio: r = DN sample (λ)/DN spectralon(λ);

Since we only measured the Lambertian surface at the beginning and at the end of each row we had to interpolate the values of DN spectralon for each sample (time). A linear interpolation between the beginning of the row and the end is a good approximation of the variability of the DN spectralon with time (Figure 6)
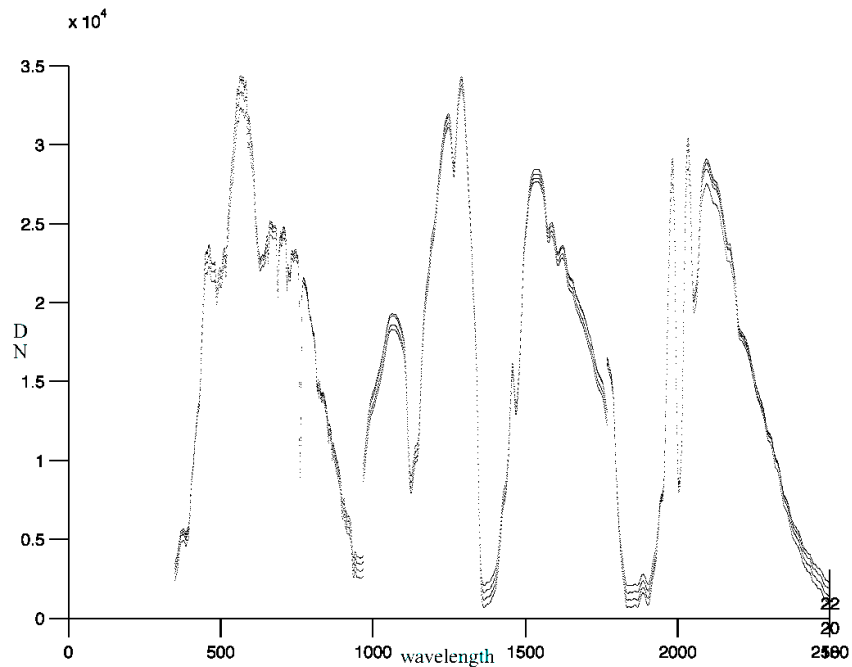

Figure 5. *Output data from the instrument plotted versus wavelength. Different curves correspond to different samples.*
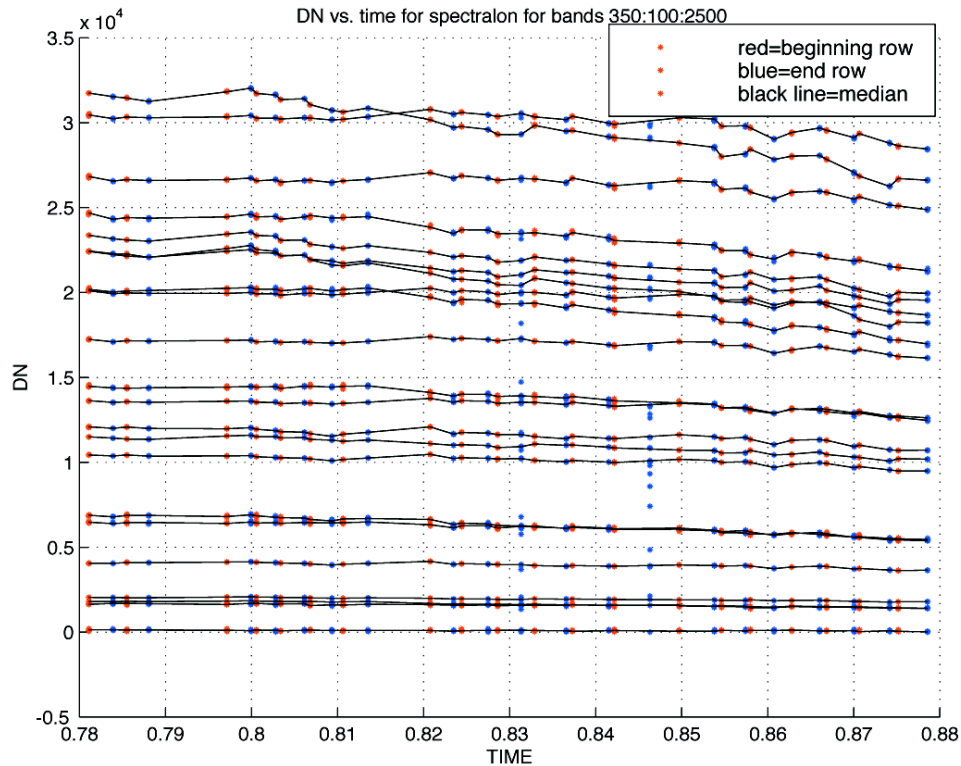
Figure 6. *Variability of the measurements of Spectralon from the beginning to the end of the experiment. Black lines correspond to the median value of the 5 measurements performed at the beginning and end of each row.*

The calculation of reflectance was performed using our own code written in Matlab 5.1. After reflectance per sample per wavelength was calculated, all the data was combined in a 3-D matrix of 20x111x2152. Two strong atmospheric absorption bands (see Figure 5) 1350-1400 and 1780-1960 were removed immediately after reflectance calculation. Using the values of reflectance we were able to compare the spectra of each sample in different ways. The analysis performed included Principal Component Analysis, Bands Ratios, Bands plotted as RGB, Ratios between samples, Cluster analysis using Euclidean distance, Comparison of absorption features and supervised Spectral Angle Mapper of full spectra and selected segments of spectral. In the next section we are focusing on the supervised Spectral Angle Mapper (SAM) and compare the results obtained from this method with the digital photography of the trench wall and with an image generated with an expedite sedimentological description of the of the samples. The SAM method was chosen among the others because it is simple, and has provided the best results so far.

9   Brief description of the Spectral Angle Mapper Algorithm

This *supervised* classification algorithm is defined by the following metric used to quantify the separation between two samples (Krause, et al, 1993):

$$\cos^{-1}\left[\frac{\sum_{b=1}^{n} i_b r_b}{\sqrt{\sum_{b=1}^{n} i_b^2 \sum_{b=1}^{n} r_b^2}}\right]$$

Where r represents the amplitude of the reference spectrum at band b and i represent the amplitude of the spectrum to be matched at band b. The angle obtained for each sample is compared with the others. Values close to zero indicate very similar spectrums and values away from zero mean that spectrum is different. If two spectra have similar angles respect to the reference sample doesn't indicate that these two samples are similar. Results of SAM analysis are shown in next section.

10 Digital photography vs. Spectral Angle Mapper

In recent years, digital photography has become one of the principal tools used to describe and record the trench exposures. During this experiment we compared a 20 x 20 pixels image of the samples created using the SAM algorithm with 1) a high resolution digital photography 2953 x 2953 pixels (150 pixels/inch) (Figure 8), 2) a 20 x 20 pixels version of the same photography created using the Pixilated Mosaic filter of Photoshop 7.0 (Figure 9) and 3) the same pixilated version as in 2 covered with a mask that only shows the sampled area of the trench wall (Figure 10).
The high resolution digital image (Figure 8) depicts a great amount of textural detail and colors that can be used to define units. But it does not give information about composition of the units. The SAM image has low resolution automatically map lithological units based on their spectral similarity (Figure 11). SAM algorithm successfully mapped the limit between fine grain sand and medium sand (Figure 12) that is not recognizable in the digital picture.
The pixilated version of the digital picture has the same resolution than the SAM image (20x20 pixels) and as can be seen on Figure 9, it only grossly shows the limits between the white sand unit and the clays. A light clay unit looks almost identical to the sand unit. When this low-resolution image is compared with the SAM image it is possible to see that for the same resolution, the SAM image provide much more information about the stratigraphy of the trench wall.

Figure 8 *high-resolution digital photographs. (2953x2953 pixels).*

Figure 9 *Pixelated 20 x 20 image created from Figure 8 digital photography. Notice that at this resolution the sands, clay boundaries look poorly defined and the light clay unit looks almost the same as the medium sand.*
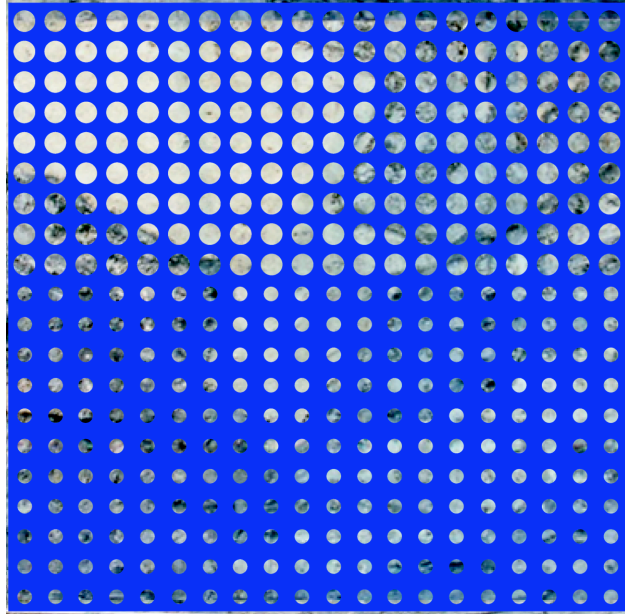
Figure 10. *High-resolution digital photography covered with a mask that resembles the sampling area. Each circle corresponds to a sample. Bigger circles represent samples taken with the metal pipe containers, small circles are PVC pipe. The area measured with the hyperspectral instrument corresponds to the area of the circles.*
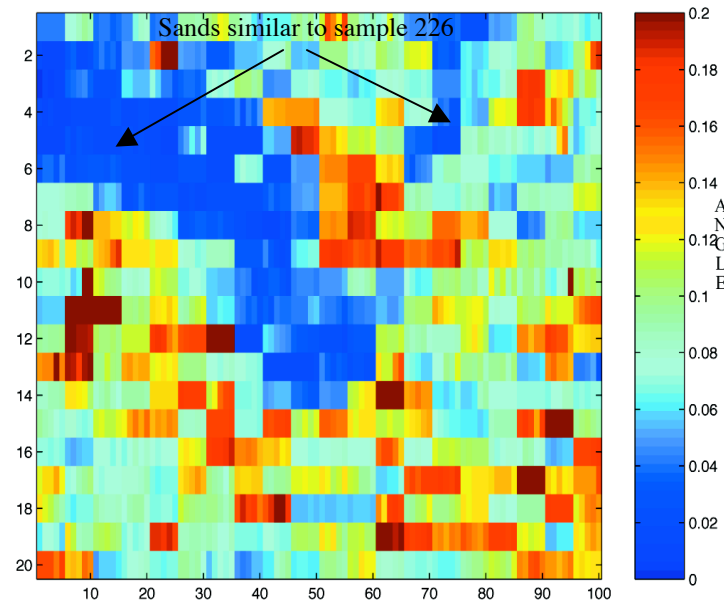

Figure 11. *Image of the hyperspectral data created with the SAM algorithm using spectra 226 (sample 41-Medium sand) as the reference material. In blue, the image shows the samples that are very similar to the spectra 226. Compare this image with Figure 13 below and notice that the image reproduced the limits of the medium sand (dark pink in figure 13) with great accuracy.*

Of course, this supervised classification does not have to measure only the similarities of the various samples with a single reference sample. Figure 12 shows a false color image where the similarity of each sample to three separate reference samples (one sand, and two clays) is measured using the spectral angle mapper. The image shows much more detail, but is quite blurred, due primarily to the large pixel size, which results in multiple lithologies being represented in a typical pixel.
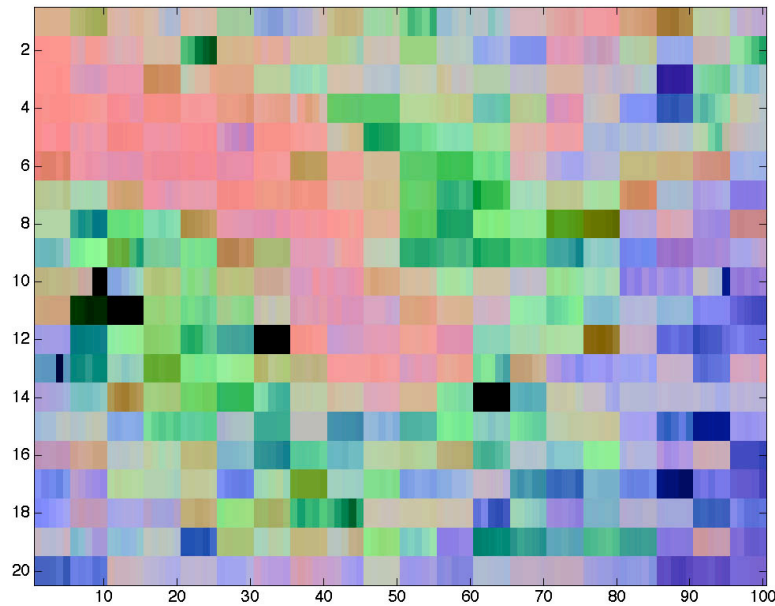

Figure 12: Image generated by combining 3 spectral angle mapper images single RGB image. The reference samples are (1) the same sand used to generate Figure 11 (pink hues) and two different clays (blue and green hues.)

This multi-sample classification can be formalized in terms of a ternary diagram as was done, for example, by Blom et al. (1980). We have not taken that step yet. This will become important in the next phase of our research

The high-resolution digital photograph covered with a mask that simulates the sampling area simulates what can be observed if only look at the surface sampled. The quality of the image generated is very poor and we can only see mayor variations. The area covered by the white medium sands can still be observed but the boundaries are poorly defined. The SAM image is providing much more information although the area measured by the hyperspectral instrument is the same as the area shown trough the mask.

11 Geological Description vs. Spectral Angle Mapper

An image generated from an expedite sedimentological description of the samples was created as a reference to be compared with the images provided by the hyperspectral processing (Figure 12). This image clearly shows the limits between sands and finer grain materials but is not as useful for variations in clay composition. When this image is compared with the SAM image (Figure 11) created specially to identify medium grain sands a excellent correlation can be observed. The SAM image not only show precisely

the location of the main contacts but also shows the limit between medium sands and finer sands, boundary that was not even described on the trench logs. These results show a very promising future for hyperspectral imagers as tools to rapidly identify and correlate different type of lithologies. Other SAM images were created for some of the clay units with equally successful results.

Figure 13. *Image based on the samples descriptions. The boundaries of the clays units shown in Figure 8 were not always observed when describing individual samples.*

In order to provide an objective assessment of the pilot experiment, we must compare images generated using comparable resolution and sampling. This includes both the "pixel" averaging. Figures 14-16 show the images that should really be compared, all seen through the sample mask. They include:

  ➢ The pixilated optical photograph (Figure 9)
  ➢ The expedite sedimentological description (Figure 13)
  ➢ The 3-sample classification false-color image (Figure 12)

These three views are shown below, together with the stratigraphy derived from field work and overlain to the digital optical photograph. Note the remarkable correspondence of the features visible in Figures 15 and 16, particularly in the top part of the sand unit, where the only indication in the optical photograph is the slight change in sand grain size. This added level of discrimination is seen in the expedite sedimentological picture, and is pulled out by the hyperspectral analysis.
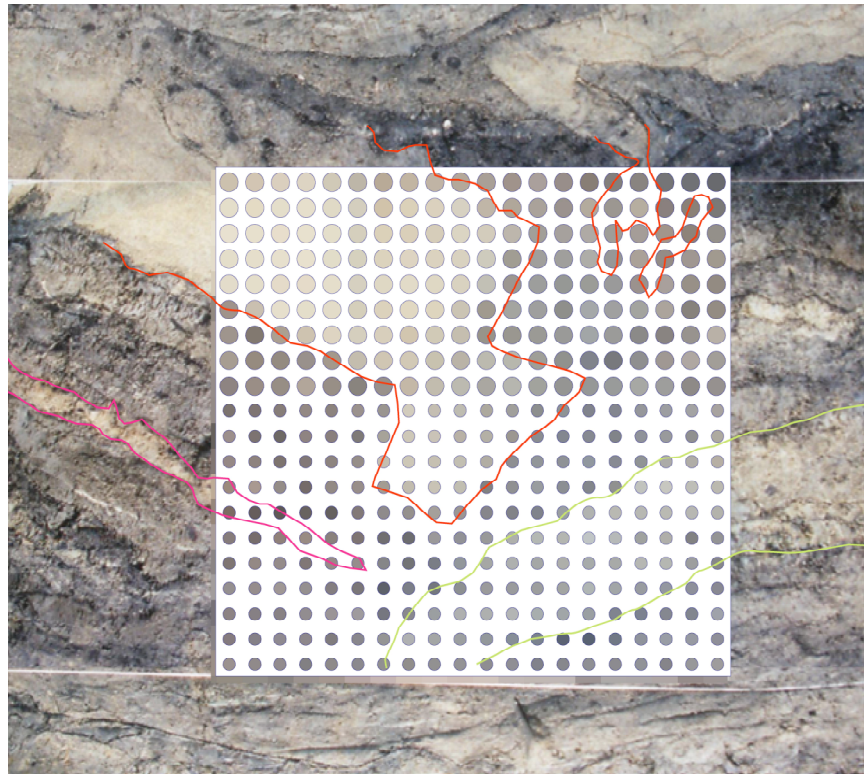
Figure 14: *Pixiliated and masked view of the high resolution optical photograph.*
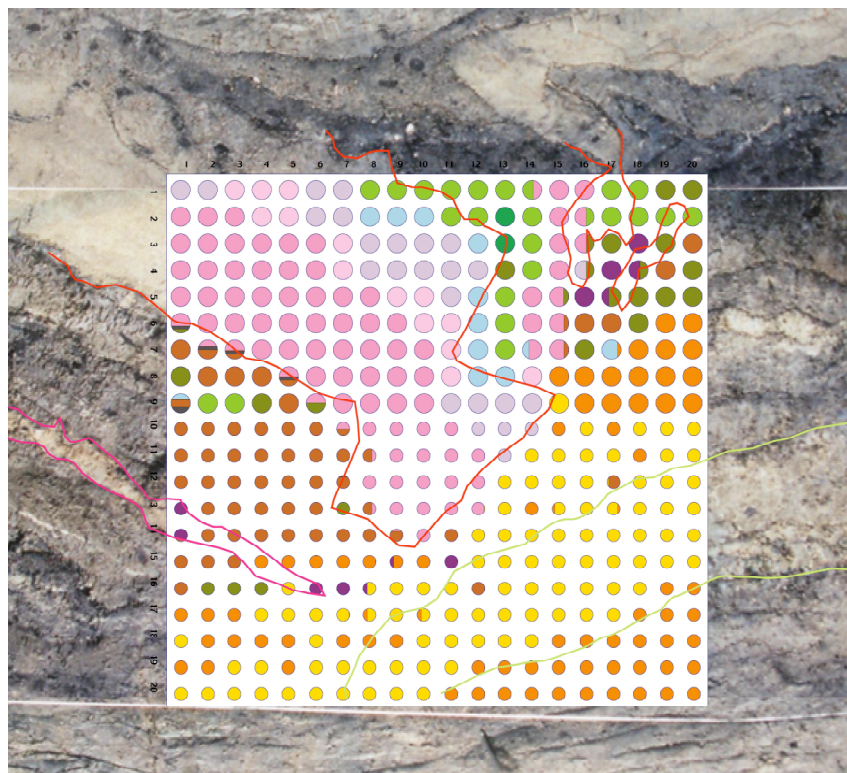

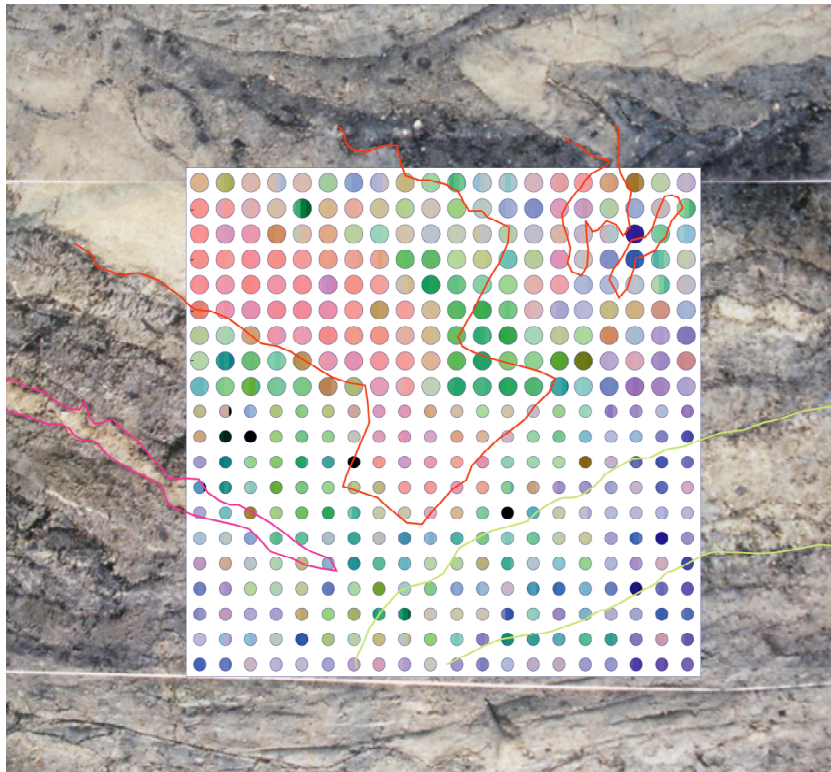Figure 15: *Masked view of the expedite sedimentological map*

Figure 16: *Masked view of the 3-sample supervised classification of the 400 sample hyperspectral data set..*

12   Discusssion:

12.1   Problems found during the experiment

Along the experiment several problems that affect the quality of the hyperspectral measurements were identified. Among those, the most important are: a) contamination of spectra with surrounding material, b) non ideal conditions of the experiment set c) salt accumulations developed on the surface of the samples d) varying moisture content of the samples, e) oxidation of the metal pipe containers, f) micro topography of the samples and shadows related g) affected natural properties of the samples (compaction, cementation, humidity content, etc) after being taking from the trench wall.
The impact of these factors in the final result is being analyzed and suggestions will be made for future experiments.

12.2   Answers to Questions posed in 2003:

The questions posed in our 2003 SCEC proposal have largely been answered, as follows:

What is the inherent stability of the measurements? The data collected on the calibration surface show excellent stability, although there is considerably more scatter in the IR data than there are in the visible band. Data collected from the samples themselves show much more scatter at times. There is occasional evidence of contamination due to stray radiation from the container (metal or PVC) and perhaps the sample box. This is largely due to the procedure which involved a hand-held instrument. There is also occasional evidence of shadow effects, again due to the experimental procedure, which is prone to variability in the illumination. However, it should be pointed out that the optical images,

taken with a digital camera and a flash, are also prone to the vagaries of uneven illumination.

What are the effects of other factors (e.g. sun angle, atmosphere) which have varied over the duration of the experiment (about 4 hours)? That turned out not to be a major issue. The long time series of calibration measurements taken from the Lambertian calibration surface shows a rather smooth variation with time as the sun angle changed through the experiment. The weather was quite steady and we did not see any major variability attributable to the atmosphere….This does not mean that such a problem will not arise in the future.

What is the best strategy to construct "processed" spectra?, The "classical" approach of dividing measured spectra by calibration spectra appears to work reasonably well for our purposes. We did find it necessary to simply remove data from two strong atmospheric absorption bands as indicated above, because of unfavorable signal-to-noise ratios in these bands, which rendered interpretation chancy at best.

What is the variability of spectra between sample? This was a rather surprising characteristic of the data: the spectra can be quite variable, even between samples which, for all intents and purposes, appear to be identical under hand lens examination. We do not fully understand all causes of variability, although we suspect a number of effects, including occasional contamination by stray radiation, occasional specular reflectance from biotite grains, and poorly controlled levels of saturation.   Sorting out these effects will require collection of additional data under controlled geometry and illumination.

Does that variability correlate usefully with the lithology and mineralogy of the samples? When using the supervised classification procedure, we find that the correlation between samples surmised to come from the same unit is quite good. This augurs well of the applicability of the method to cross-trench comparisons. However, as pointed out already, we need to firm up all protocol issues before this conclusion is confirmed.

What are the optimal spectral bands for this application, in terms of number, center frequencies and widths? We have noticed a greater level of discrimination in the infrared band than in the optical. In fact, as described above, the detailed stratigraphy derived by eye-examination of the sample box depends largely on texture and grain-level interpretation of the observations. The very coarse sampling of the section, and the large (~2cm) "pixel" size of our data set greatly reduces the sensitivity of spectral data to micro-structure and fabric. This is a question that can only be answered with additional data.

13 Conclusions

The results obtained with the Spectral Angle Mapper algorithm show extremely promising results for a hyperspectral imager. We are working on more sophisticated algorithms that can give us a better separation of the clays and other units with characteristic features. Besides the low resolution image generated from a coarse grid sampling, the experiment showed that the use of hyperspectral technology can provide

much more information than a regular digital photography (compare figures 9 and 11) and provide valuable quick lithological information (compare figures 11 and 12) that at present day can only be acquired with a detailed geological (by hand) description. We conclude that an high resolution Hyperspectral Imager can provide the ultimate tool for trench exposures logging.

14 Bibliography

Adams, J. B., Smith, M. O., and Johnson, P.E., 1986, "Spectral mixture modeling: A new analysis of rock and soil types at the Viking Lander 1 site." In *Journal of Geophysical Research*, **91**(B8), pp. 8090-8112.

Baugh, W. M., Kruse, F. A., & Atkinson Jr., W. W.,1998, Quantitative geochemical mapping of ammonium minerals in the southern Ceda Mountains, Nevada, using the Airborn Visible/Infrared Imaging Spectrometer (AVIRIS). Remote Sensing of Environment, 65, 292– 308.

Blom, Ronald, G., Michael . Abrams and Herbert, G. Adams, 1980, Spectral Reflectance and Discrimination of Plutonic Rocks in the 0.45—2.45 μm Region, *J. Geophys. Res.* ,**83**, 2638-2648.

Clark, R. N., King, T. V. V., Klejwa, M., & Swayze, G. A. (1990). High spectral resolution reflectance spectroscopy of minerals. Journal of Geophysical Research, 95(B8), 12:653 – 12:680.

Cloutis, E. A. (1996). Review article, hyperspectral geological remote sensing:evaluation of analytical techniques. International Journal of RemoteSensing, 17(12), 2215–2242.

Elvidge, C. D., 1990, "Visible and infrared reflectance characteristics of dry plant materials." In International Journal of Remote Sensing, vol. 11(10), pp. 1,775-1,795.

Emslie A. and Aaronson J. (1973) Spectral reflectance and emittance of particulate materials 1: Theory. Appl. Opt, 12, 2563-2572

Farrand, W. H., Singer, R. B., & Mereinyi, E. (1994). Retrieval of apparent surface reflectance from AVIRIS data a comparison of empirical line, radiative transfer, and spectral mixture methods. Remote Sensing of Environment, 47(3), 311 –321.

Korb, A. R., Dybwad, P., Wadsworth, W., and Salisbury, J. W., 1996, Portable FTIR spectrometer for field measurements of radiance and emissivity, *Applied Optics*, **35**, 1,679-1,692.

Kruse, F.A., Lefkoff, A.B., Boardman, J.W., Heidebrecht, K.B., Shapiro, A.T., Barloon, P.J., and Goetz, A.F.H., 1993,. The Spectral Image Processing System (SIPS) - Interactive Visualization and Analysis of Imaging Spectrometer Data, *Remote Sensing of Environment*, **44**:145-163.

Goetz, A. F. H., Vane, G., Solomon, J. E., & Rock, B. N., 1985, Imaging spectrometry for Earth remote sensing. *Science*, **228**, 1147– 1153.

Green, A. A., Berman, M., Switzer, P., & Craig, M. D., 1988, A trans-formationfor ordering multispectral data in terms of image quality withimplications for noise removal. *IEEE Transactions on Geoscience and Remote Sensing*, **26**(1), 65–74.

Green, R. O., Eastwood, M. L., Sarture, C. M., Chrien, T. G., Aronsson, M., Chippendale, B. J., Faust, J. A., Pavri, B. E., Chovit, C. J., Solis, M.,Olah, M., & Williams, O.,1998, Imaging spectroscopy and the Air-borne Visible/Infrared Imaging Spectrometer (AVIRIS). *Remote Sensing of Environment*, **65**, 227– 248.

Hapke B., 1981, Bidirectional reflectance spectroscopy, 1 Theory, *J. Geophys. Res*, **86** 3039-3054

Hapke B.,1984, Bidirectional reflectance spectroscopy 3. Correction for macroscopic roughness. *Icarus* **59**, 41-59

Hapke B.,1986, Bidirectional reflectance spectroscopy, 4 the extinction coefficient and the opposition effect. *Icarus*, **67**, 264-280.

Lumme K. and Bowell E.,1981, Radiative transfer in the surfaces of airless bodies: I theory. *Astron. J.* **86** 1694-1704

Hunt, G. R. 1977, Spectral signatures of particulate minerals in the visibleand near-infrared. *Geophysics*, **42**, 501–513.

Hunt, G. R., & Salisbury, J. W., 1970, Visible and near-infrared reflectancespectra of minerals and rocks, I: silicate minerals. *Modern Geology*, **1**,219– 228.

Hunt GR., 1979, Near-infrared (1.3 –2.4 _ Spectra of alteration minerals: Potential for use in remote sensing., *Geophys*, ;**44**:1974 –1986.

Kruse, F. A., 1988, Use of Airborne Imaging Spectrometer data to map minerals associated with hydrothermally altered rocks in the northern Grapevine Mountains, Nevada and California. *Remote Sensing of Environment*,**24**, 31– 51.

Mustard, J. F., & Pieters, C. M., 1987, Abundance and distribution of ultramafic microbreccia in Moses Rock dike: quantitative application of mapping spectroscopy. *J. Geophys. Res.*, **92**,E617–E626.

Salisbury, J. W., D'Aria, D. M., and Jarosevich, E., 1991a, Mid-infrared (2.5-13.5 micrometers) reflectance spectra of powdered stony meteorites, *Icarus*, **92**, 280-297.

Salisbury J and Eastes J., 1985, The effect of particle size and porosity on spectral contrast in the mid-infrared. *Icarus*, **64**, 586-588.

Salisbury, J. W., Wald, A., and D'Aria, D. M., 1994, Thermal-infrared remote sensing and Kirchhoff?s law 1. Laboratory measurements, *J. Geophys. Res.*, **99**, pp. 11,897-11,911.

Spencer J., 1990, A rough-surface thermophysical model for airless planets. *Icarus*, **83**, 27-38

Vincent R. and Hunt G.,1968, Infrared reflectance from mat surfaces. *Appl. Opt,* **7**, 53-59